Mon. Not. R. Astron. Soc. **317**, 1029–1040 (2000)

The effect of radiative cooling on the X-ray properties of galaxy clusters

F. R. Pearce,[1]★ P. A. Thomas,[2] H. M. P. Couchman[3] and A. C. Edge[1]

[1]*Department of Physics, University of Durham, Durham DH1 3LE*
[2]*Astronomy Centre, CPES, University of Sussex, Falmer, Brighton BN1 9QJ*
[3]*Department of Physics and Astronomy, McMaster University, Hamilton, Ontario L8S 4M1, Canada*

Accepted 2000 June 9. Received 2000 May 12; in original form 1999 July 5

ABSTRACT

In this paper, we investigate the effect of cooling on the X-ray properties of galaxy clusters. We have performed *N*-body, hydrodynamical simulations both with and without the effects of radiative cooling, but neglecting the effects of star formation and feedback. We show that radiative cooling produces an inflow of high-entropy gas from the outer parts of the cluster, thus *raising* the cluster temperature and *decreasing* the X-ray luminosity. With radiative cooling clusters are on average from three to five times less luminous in X-rays than the same clusters simulated without cooling. However, we do not produce a large constant-density core in either the gas or the dark matter distributions. Our results contradict previous work in which cooling raises the X-ray luminosity and deposits an unreasonably large amount of mass in the central cluster galaxy. We achieve this by selecting our numerical resolution in such a way that a reasonable fraction of the baryonic material cools and by decoupling the hot and cold gas in our simulations, a first step towards modelling multiphase gas. We emphasize that globally cooling a sensible amount of material is vital and the presence or absence of massive central concentrations of cold baryonic material has a dramatic effect upon the resultant X-ray properties of the clusters.

Key words: hydrodynamics – methods: numerical – galaxies: clusters: general – cosmology: miscellaneous.

1 INTRODUCTION

Clusters of galaxies are the largest virialised structures in the Universe, evolving rapidly at recent times in many popular cosmological models. Even at moderate redshifts the number of large dark matter haloes in a cold dark matter (CDM) Universe with a significant, positive cosmological constant is higher than in a standard cold dark matter (SCDM) Universe and it is precisely because both the number density and size of large dark matter haloes evolve at different rates in popular cosmological models that observations of galaxy clusters provide an important discriminator between rival cosmologies.

The advent of X-ray satellites opened up a whole new area in observational astronomy. Hot gas, typically at temperatures of 10^7–10^8 K, sitting in the deep potential wells of galaxy clusters emits radiation via thermal bremsstrahlung. This emission is heavily biased towards the central regions of the cluster because the flux is weighted as the gas density squared. Given the gas temperature and the X-ray surface brightness, the gas column density and a spherically symmetric gas density profile can be estimated. If the hot gas is assumed to reside close to hydrostatic equilibrium within the dark matter halo, the underlying dark matter density distribution can be derived.

★ E-mail: F.R.Pearce@durham.ac.uk (FRP)

Since the early work of Abramopoulos & Ku (1983) and Jones & Forman (1984) on the radial density profiles of large galaxy clusters, debate has raged about the presence or absence of large, $\sim 250\,h^{-1}$ kpc, constant-density cores in the X-ray emitting gas. Unfortunately X-ray imaging is notoriously difficult because of the inherent large beam size. In addition, the centre of the emission region is not easy to determine and any centring error also acts to smooth out any central increase when the results are azimuthally averaged and plotted as a radial profile (Beers & Tonry 1986). More recent high-resolution images of several clusters have helped to resolve this controversy. Some galaxy clusters do indeed appear to exhibit a large, resolved core but others have a much smaller core, close to the resolution threshold of the instrument. Both White, Jones & Forman (1997) (who studied 207 clusters imaged by the Einstein observatory) and Peres et al. (1998) (who looked at *ROSAT* observations of the flux-limited sample of clusters provided by Edge et al. 1990) suggest that this dichotomy relies on the presence or absence of a cooling flow. Clusters with a cooling flow appear to have small cores (around $50\,h^{-1}$ kpc) whilst clusters without cooling flows have much larger cores. The work of Allen (1998) on the discrepancy between the large X-ray core radii and the small core radii deduced from strong lensing observations (e.g. Kneib et al. 1996) also reached the conclusion that cooling-flow-type clusters had small core radii in their matter distributions. Because the X-ray

flux rises as the local density squared, the total X-ray emission from a cluster is very sensitive to the central density.

High-resolution *N*-body simulations of galaxy clusters (Moore et al. 1998) produce a radial dark matter profile that has no core. The radial profile continues to rise until the resolution threshold is reached, well within the required radius if the gas is to trace the dark matter and still reproduce the X-ray observations. The production of a central constant density dark matter core has been a long-standing problem for collisionless dark matter simulations (Pearce, Thomas & Couchman 1993; Navarro & White 1994), although in previous work the resolution threshold was still close to the observed core sizes and so until the latest high-resolution studies this was still a tentative result.

Recently, several groups have tried to reconstruct the radial temperature profile of galaxy clusters. Markevitch et al. (1998) used *ASCA* data from 30 clusters and concluded that the temperature falls steeply at large radii. However, Irwin, Bregman & Evrard (1999) analysed *ROSAT* Position Sensitive Proportional Counter (PSPC) images of 26 clusters and concluded that the radial temperature profiles were generally flat out to the virial radius.

The inclusion of a gaseous component into simulations allows the previously assumed relationship between the gas and the dark matter to be derived directly. The first study of this type (Evrard 1990) was carried out without the effects of radiative cooling but reproduced well many theoretical predictions such as a bias between the dark matter and the baryonic material. Similar non-cooling simulations have proved popular (Bryan et al. 1994; Cen & Ostriker 1994; Kang et al. 1994; Navarro, Frenk & White 1995; Bartelmann & Steinmetz 1996; Eke, Navarro & Frenk 1998; Bryan & Norman 1998) and such a simulation formed the basis of the Santa Barbara project in which a dozen groups simulated the formation of the same galaxy cluster (Frenk et al. 1999).

Extending this work to include a dissipative component has proved difficult because the formation of galaxies introduces many additional physical effects. Metzler & Evrard (1994) and Evrard, Metzler & Navarro (1996) circumvented this by introducing a galactic component by hand into a simulation that did not follow radiative cooling of the gas to study the effects of feedback on the cluster profile. Fully consistent attempts to follow the radiative cooling of the hot intracluster gas have only recently been achievable because of the extra computational overhead involved. Early attempts to include the effects of radiative cooling (Thomas & Couchman 1992; Katz & White 1993; Evrard, Summers & Davis 1994; Frenk et al. 1996) either suffered from poor resolution, focussed on the galactic population or suffered from overmerging effects.

In a now classic paper Katz & White (1993) examined the effect of radiative cooling on the X-ray profile of a single galaxy cluster, a study repeated recently by Lewis et al. (2000). Their simulated cluster has properties that are not observed: a Virgo-sized cluster with a supermassive central galaxy and an enormous $400\,\mathrm{M}_{\odot}\,\mathrm{yr}^{-1}$ associated cooling flow. As they point out, massive brightest cluster galaxies of this size are observed within the Universe, as are massive cooling flows; however, they fail to stress their rarity, particularly in objects of similar size to the Virgo cluster. More recently Suginohara & Ostriker (1998) simulated a different cluster and also produced an object which has properties they themselves admit are unobserved – 'The high resolution simulation resulted in a gas density profile steeply rising toward the center, with consequent very high X-ray luminosity; however, these properties are not observed'. They suggest that feedback of energy from supernovae might account for the discrepancy. In this paper, we obtain quite different results because, unlike previous studies, a realistic fraction of the baryonic material has cooled to form galaxies. Large, bright central cluster galaxies can have a dramatic effect on the cluster potential and, consequently, the X-ray properties. A reasonable treatment of these objects is extremely important in studies of this type. To prevent too much material cooling to form the central object within each halo we employ a modified form of smoothed-particle hydrodynamics – this will be described further in Section 2, below.

If the effects of cooling are included in the models then one might expect the entropy of the intracluster medium to decrease. Paradoxically, several mechanisms have been suggested that may produce large, constant-density gas cores by *raising* the entropy of the gas at the centre of the cluster:

(i) Radiative cooling is very efficient in small dark matter haloes because the cooling time is less than the dynamical time (White & Rees 1978). These knots of cold, dense gas can be equated with protogalaxies and, as they are dense and collapsing, they may be reasonably expected to produce stars (Katz 1992). Star formation leads to energy feedback into the interstellar medium via supernovae explosions (Katz 1992; Mihos & Hernquist 1994; Navarro & White 1994; Gerritsen & Icke 1997). Unless the gas immediately recools, this heating acts to increase the entropy of the surrounding material, pushing it on to a higher adiabat and preventing it settling to the very high densities and temperatures required for it to trace the underlying dark matter (Wu, Fabian & Nulsen 1998).

(ii) The presence of galaxies orbiting within the cluster potential acts to stir up the gas, heating it as friction and turbulence dissipate the galaxies' velocity, simultaneously producing velocity and spatial bias in the galaxy distribution (Frenk et al. 1996). This effect is most pronounced in the centre of the cluster.

(iii) A third mechanism for producing a core is that radiative cooling of the gas at the centre of each potential well acts as a drain on the low entropy material (which cools preferentially). If the remaining gas cannot cool rapidly enough, a core would develop because only high-entropy material remains, an effect postulated in the first paper to include radiative cooling (Thomas & Couchman 1992) and later reiterated by Waxman & Miralda-Escude (1995); Bower (1997). It is this mechanism that we investigate in this paper. We show that the entropy of the intracluster medium is indeed increased, that this leads to a greatly reduced X-ray luminosity, but that it does *not* give a large, constant-density core.

The remainder of this paper is laid out as follows: in Section 2 we present the large hydrodynamical simulations, both with and without the effects of radiative cooling, that we have performed; in Section 3 we extract radial density and temperature profiles for the 20 largest galaxy clusters within each simulation and contrast the profiles with the underlying dark matter distribution; this is followed in Section 4 by a discussion of our findings.

2 THE SIMULATIONS

The simulations that we have carried out use the adaptive particle–particle, particle–mesh ($\mathrm{AP^3M}$) method (Couchman 1991) coupled to the smoothed particle hydrodynamics (SPH) technique (Gingold & Monaghan 1977; Lucy 1977) to follow

Table 1. The main parameters for each cosmology. The parameters for the cooling and non-cooling runs were identical.

Cosmology	ΛCDM	SCDM
Ω	0.3	1.0
Λ	0.7	0.0
$\Omega_{\rm b}$	0.03	0.06
σ_8	0.9	0.6
h	0.7	0.5
boxsize (h^{-1} Mpc)	70	50
$M_{\rm dm}$ ($h^{-1}\,{\rm M}_\odot$)	1.4×10^{10}	1.6×10^{10}
$M_{\rm gas}$ ($h^{-1}\,{\rm M}_\odot$)	1.4×10^{9}	1.0×10^{9}
soft (h^{-1} kpc)	10.	10.
$Z_{\rm met}$ (solar)	0.3	0.3

2 million gas and 2 million dark matter particles in a box of side 100 Mpc (Couchman, Thomas & Pearce 1995; Pearce & Couchman 1997).

We have performed simulations in two types of flat CDM cosmology, one standard (SCDM) and one with a cosmological constant (ΛCDM), with the same parameters assumed by Jenkins et al. (1998) ($\Omega = 1.0, \Lambda = 0.0, h = 0.5, \sigma_8 = 0.6$ for the former and $\Omega = 0.3, \Lambda = 0.7, h = 0.7, \sigma_8 = 0.9$ for the latter). The baryon fraction was set from big bang nucleosynthesis constraints, $\Omega_{\rm b}h^2 = 0.015$ (Copi, Schramm & Turner 1995) and we have assumed an unevolving gas metallicity of 0.3 times the solar value. These parameters produce a gas mass per particle of $2\times10^9\,{\rm M}_\odot$ in each case and are summarized in Table 1. The dark matter mass is only slightly lower than that given by Steinmetz & White (1997) (their equation 9, but note that there is a typographical error) at which artificial 2-body heating balances radiative cooling. Thus we expect there to be some numerical heating in our simulations. However, as we have chosen to neglect real heat sources, such as supernovae in galaxies, this is of little importance and does not affect our conclusions, which concern the differences between runs with and without radiative cooling.

Since we smooth over 32 SPH particles, the smallest gaseous object that can be effectively resolved has a mass of $6.4\times10^{10}\,{\rm M}_\odot$ We employ a comoving β-spline gravitational softening equivalent to a Plummer softening of $10\,h^{-1}$ kpc for redshifts $0 < z < 1.5$ (2.5 for ΛCDM) – at earlier times the softening has a fixed physical size, with the minimum SPH resolution set to match this. We note that a spatial resolution of $10\,h^{-1}$ kpc is over twice the typical scalelength of elliptical galaxies and this may lead to enhanced tidal disruption, drag and merging within the largest clusters of objects. However, the force softening cannot be reduced further without introducing 2-body effects. A smaller softening would also lead to a further increase in the number of time-steps required; we already require around 10 000 for each cooling run.

In addition to these two simulations, which both included the effects of radiative cooling, we repeated the ΛCDM model without cooling. This simulation has input parameters close to those used by Eke, Navarro & Frenk (1998) who used the same cosmology and the resultant clusters look very similar and exhibit similar X-ray properties (see Fig. 7 for a comparison).

The properties of the galaxies in the two simulations with radiative cooling have been described in Pearce et al. (1999) (and in preparation). They clearly demonstrate an acceptable match to both the spatial and luminosity distributions of observed galaxies. This was achieved by employing three numerical approximations: a mass-resolution of $6.4\times10^{10}\,{\rm M}_\odot$ below which objects cannot cool efficiently, a length-resolution (i.e. softening) of $10\,h^{-1}$ kpc, and decoupling of the hot, halo gas from the cold galactic gas. Improving the mass and/or length resolution would increase the fraction of cold gas in our simulations, producing galaxies that were too luminous to match the observations. This would then necessitate the introduction of feedback mechanisms that would overcomplicate our model.

Table 2. Data for the 20 largest clusters (by mass) in the ΛCDM run without cooling. Quoted are the cluster number, the virial mass in units of $10^{14}\,h^{-1}\,{\rm M}_\odot$, the virial radius in h^{-1} Mpc, the value of the substructure parameter defined in the text (a larger number implies more substructure), the number of dark matter particles within the virial radius, the number of gas particles within this radius, the emission weighted mean temperature (in keV k^{-1}) and the bolometric X-ray luminosity in units of $10^{43}\,{\rm erg\,s^{-1}}\,h^{-2}$.

Run	$M_{\rm v}$	Virial rad.	substruct.	$N_{\rm dm}$	$N_{\rm hotgas}$	$T_{\rm X}$	$L_{\rm X}$
Λnc1	8.54	1.97	0.023	63175	54842	6.31	49.3
Λnc2	3.07	1.40	0.086	22643	18175	2.61	3.43
Λnc3	2.54	1.31	0.071	18770	16094	2.04	3.39
Λnc4	1.82	1.17	0.097	13431	11218	1.55	2.32
Λnc5	1.53	1.10	0.073	11256	9642	1.92	4.02
Λnc6	1.53	1.10	0.033	11235	9072	1.71	2.64
Λnc7	1.43	1.08	0.013	10552	9262	2.12	4.26
Λnc8	1.24	1.03	0.018	9138	7780	1.89	2.96
Λnc9	1.19	1.01	0.083	8766	7201	1.44	0.69
Λnc10	1.10	0.99	0.018	8091	6414	1.49	1.63
Λnc11	1.09	0.99	0.032	8054	7204	1.84	2.44
Λnc12	1.03	0.96	0.020	7573	6250	1.59	3.09
Λnc13	0.99	0.96	0.008	7351	6187	1.97	3.33
Λnc14	0.98	0.95	0.006	7227	5956	1.65	1.43
Λnc15	0.92	0.93	0.012	6829	5542	1.43	0.98
Λnc16	0.83	0.90	0.008	6169	4958	1.47	1.34
Λnc17	0.83	0.90	0.241	6130	4740	0.91	0.47
Λnc18	0.83	0.90	0.035	6082	5038	1.36	1.14
Λnc19	0.78	0.88	0.030	5804	5321	1.41	1.01
Λnc20	0.76	0.87	0.027	5636	4456	1.27	1.37

Decoupling the hot halo gas is a new innovation that we feel vastly improves the ability of SPH to model fluids in which there are large density contrasts. Without it, hot gas particles have their density overestimated in the vicinity of cold gas and too much material cools to form the central galaxy. Normal cooling of the intracluster medium at temperatures above 10^5 K is still handled correctly and galaxy–galaxy mergers and viscous drag on the galaxies as they orbit within the halo are retained. As Pearce et al. (1999) show, such a procedure produces a set of galaxies that fit the local *K*-band number counts of Gardner et al. (1997). The brightest cluster galaxies contained within the largest haloes are not excessively luminous for a volume of this size, unlike those found in previous work (Katz & White 1993; Lewis et al. 2000). The fraction of the baryonic material that cools into galaxies within the virial radius of the large haloes in our simulation is listed in Tables 3 and 4 and is typically around 20 per cent. This is much less than the unphysically high value of 40 per cent reported by Katz & White (1993). Decoupling of the hot phase produces a galactic population and cold gas fraction that is well matched to the observations.

3 RESULTS

3.1 Extracting objects

For the purposes of this paper we are interested in only the largest objects within each simulation, as only these contain sufficient

Table 3. Data for the 20 largest clusters (by mass) in the ΛCDM run which includes cooling. Quoted are the cluster number, the number of the matching cluster in the ΛCDM run without cooling (if one exists), the virial mass in units of $10^{14}\,h^{-1}\,\mathrm{M}_{\odot}$, the virial radius in $h^{-1}\,\mathrm{Mpc}$, the value of the substructure parameter defined in the text, the number of dark matter particles within the virial radius, the number of gas particles above and below 12 000 K within this radius, the number of cold particles within $100\,h^{-1}\,\mathrm{kpc}$ of the centre, the fraction of the baryonic material within the virial radius that has been able to cool, the emission weighted mean temperature (in $\mathrm{keV}\,k^{-1}$) and the bolometric X-ray luminosity in units of $10^{43}\,\mathrm{ergs\,s^{-1}}\,h^{-2}$.

Cluster	Match	M_{v}	Virial rad.	substruct.	N_{dm}	N_{hotgas}	N_{coldgas}	N_{gal}	cold fraction	T_{X}	L_{X}
Λ1	1	8.75	1.98	0.025	64516	46928	7528	2894	0.14	4.64	14.2
Λ2	2	2.79	1.35	0.103	20612	13485	3939	1578	0.23	3.41	1.10
Λ3	3	2.58	1.31	0.044	19070	12035	4109	1319	0.25	2.58	1.04
Λ4	4	1.60	1.12	0.182	11855	7409	2467	1082	0.25	2.22	0.61
Λ5	7	1.50	1.10	0.014	11118	7340	2262	1253	0.24	0.87	2.75
Λ6	5	1.48	1.09	0.008	10936	7369	2148	1338	0.23	2.09	1.30
Λ7	6	1.29	1.04	0.009	9526	6649	1613	1241	0.20	2.50	1.28
Λ8	–	1.22	1.02	0.020	8978	4901	2500	1074	0.34	1.59	0.21
Λ9	8	1.21	1.02	0.049	8916	5252	2137	1182	0.29	2.57	0.29
Λ10	10	1.14	1.00	0.015	8397	5345	1764	773	0.25	1.97	0.35
Λ11	9	1.11	0.99	0.038	8213	4573	1770	1172	0.28	1.91	0.23
Λ12	13	0.98	0.95	0.004	7231	5097	1232	1031	0.19	2.18	0.82
Λ13	12	0.98	0.95	0.002	7213	4630	1327	979	0.22	1.94	0.40
Λ14	11	0.96	0.94	0.050	7074	4154	1413	1041	0.25	1.73	0.23
Λ15	14	0.92	0.93	0.189	6836	4359	1602	648	0.27	1.74	0.32
Λ16	16	0.92	0.93	0.037	6766	4156	1533	807	0.27	1.64	0.27
Λ17	18	0.87	0.91	0.073	6386	3713	1704	523	0.31	1.03	0.22
Λ18	–	0.82	0.89	0.192	6022	3346	1707	348	0.34	1.34	0.21
Λ19	15	0.76	0.87	0.043	5578	3155	1577	828	0.33	1.38	0.30
Λ20	–	0.75	0.87	0.179	5539	3264	883	332	0.21	2.00	0.18

Table 4. Data for the 20 largest clusters (by mass) in the SCDM run which includes cooling. Quoted are the cluster number, the number of the matching cluster in the ΛCDM run without cooling (if one exists), the virial mass in units of $10^{14}\,h^{-1}\,\mathrm{M}_{\odot}$, the virial radius in $h^{-1}\,\mathrm{Mpc}$, the value of the substructure parameter defined in the text, the number of dark matter particles within the virial radius, the number of gas particles above and below 12 000 K within this radius, the number of cold particles within $100\,h^{-1}\,\mathrm{kpc}$ of the centre, the fraction of the baryonic material within the virial radius that has been able to cool, the emission weighted mean temperature (in $\mathrm{keV}\,k^{-1}$) and the bolometric X-ray luminosity in units of $10^{43}\,\mathrm{ergs\,s^{-1}}\,h^{-2}$.

Cluster	Match	M_{v}	Virial rad.	substruct.	N_{dm}	N_{hotgas}	N_{coldgas}	N_{gal}	cold fraction	T_{X}	L_{X}
S1	1	9.65	1.67	0.069	58750	50740	3490	1286	0.06	7.48	6.55
S2	2	4.15	1.26	0.144	25181	18881	2494	805	0.12	4.47	1.09
S3	3	2.83	1.11	0.234	17171	13385	1942	522	0.13	2.91	0.62
S4	4	2.05	0.99	0.071	12452	9458	1304	475	0.12	2.27	0.43
S5	9	1.89	0.97	0.082	11467	8775	1408	461	0.14	2.42	0.36
S6	5	1.85	0.96	0.038	11221	8489	1201	631	0.12	2.10	1.07
S7	6	1.59	0.91	0.014	9653	6782	1373	480	0.17	2.38	0.19
S8	8	1.49	0.89	0.020	9020	6696	915	683	0.12	1.74	0.43
S9	7	1.39	0.87	0.015	8423	6979	774	666	0.10	2.91	0.63
S10	–	1.37	0.87	0.025	8319	5978	966	596	0.14	2.89	0.24
S11	11	1.34	0.86	0.025	8128	5896	1134	600	0.16	2.50	0.21
S12	14	1.23	0.84	0.117	7476	5737	894	384	0.13	2.29	0.31
S13	13	1.21	0.83	0.025	7355	5965	643	466	0.10	3.18	0.31
S14	10	1.19	0.83	0.007	7244	5464	729	442	0.12	2.53	0.21
S15	12	1.02	0.79	0.052	6204	4533	812	244	0.15	1.55	0.14
S16	–	1.01	0.78	0.030	6116	4364	862	371	0.16	1.61	0.10
S17	–	0.97	0.77	0.035	5874	4423	671	454	0.13	2.26	0.12
S18	20	0.93	0.76	0.097	5656	3878	888	230	0.19	2.68	0.16
S19	15	0.86	0.74	0.042	5196	3639	775	250	0.18	1.66	0.10
S20	17	0.86	0.74	0.008	5186	4184	445	370	0.10	2.16	0.15

mass to produce the deep potential wells required to retain hot, X-ray emitting gas. We centre each cluster on the peak of the hot gas density, a position that coincides with the centre of the X-ray emission. This prevents the introduction of an artificial constant-density core, which may arise with any other choice of centre – for clusters with significant substructure the centre-of-mass can lie a long way from the centre of the X-ray emission.

The virial radius for each of our clusters was defined as the spherical region, surrounding each cluster centre, which enclosed an overdensity of 178 for SCDM and 324 for ΛCDM (Eke, Cole & Frenk 1996). Each catalogue was then cleaned by ordering it in size and deleting the smaller of any overlapping clusters. The 20 most massive clusters in each of the catalogues were then used for the work presented here. The properties of the clusters are presented in Tables 2–4. The 16 largest clusters found in the non-cooling simulation are found in the list of the 20 largest clusters in the other two models. The index of the matching cluster from the non-cooling run is given in Tables 3 and 4.

Each of the extracted clusters was checked for substructure by comparing the centre of the X-ray emission to the median position

of the particles within the virial radius, a statistic that has been shown to be a useful indicator of the presence of substructure by Thomas et al. (1998). The results of this test are shown in Tables 2–4. All the clusters with an offset of more than 7 per cent of the virial radius (six in each case) were noted and are shown as dotted lines on Figs 1 and 3–6 and as open symbols on Fig. 7.

3.2 Dark matter density profiles

The radial dark matter density profiles for the 20 largest objects in each cosmology are shown in Fig. 1. Shown is the mean density within spherical shells, the innermost shell plotted in the figure containing at least 64 particles. The dark matter profiles of those clusters without significant substructure are similar within each cosmology. In the non-cooling run, the innermost bin of each density profile shows a flattening. This is a resolution effect: the radial extent of the bin has to be very large in order to accommodate 64 particles.

Both gas and dark matter density profiles for the largest object in each of the runs are shown in Fig. 2. The dark matter profile for the ΛCDM run without cooling is reasonably well fit by an NFW profile (Navarro, Frenk & White 1997). With cooling the dark matter density profile of the clusters is not well fit by the NFW formula, because the asymptotic slope in the central regions is steeper than -1. This is because, once cooling has been implemented, the large galaxy that forms at the centre of each cluster acts to draw in more dark matter and steepen the profile significantly in the inner regions. A similar effect is seen for most of the other clusters, although in the cooling run several show a drop in density in the innermost bin. This indicates that the peak X-ray emissivity sometimes comes from a galaxy that is not located at the centre of the cluster.

3.3 Gas entropy profiles

Gas entropy profiles (and also density and temperature profiles, below) were obtained using only those particles with a temperature exceeding 12 000 K. Typical gas temperatures exceed 10^7 K for haloes in this mass range and we wish to exclude cold gas which lies within galaxies or recently tidally disrupted objects. If the cold material were included, there would be a large density spike at the centre of each of the clusters (which all have a central galaxy). This object does not contribute to the X-ray emission because the material it contains is very cold compared to the surrounding hot halo (although the increased depth of the local potential can help to confine dense, hot gas, which can affect the bolometric X-ray emission). The specific entropy profile is shown in Fig. 3. We plot the quantity $(T/\mathrm{K})/(\rho/\bar{\rho})^{2/3}$, where T is the temperature and ρ the density, measured in units of the mean gas density, $\bar{\rho}$.

Let us contrast the results for the ΛCDM runs with and without cooling. First, note that the entropy at the virial radii is very

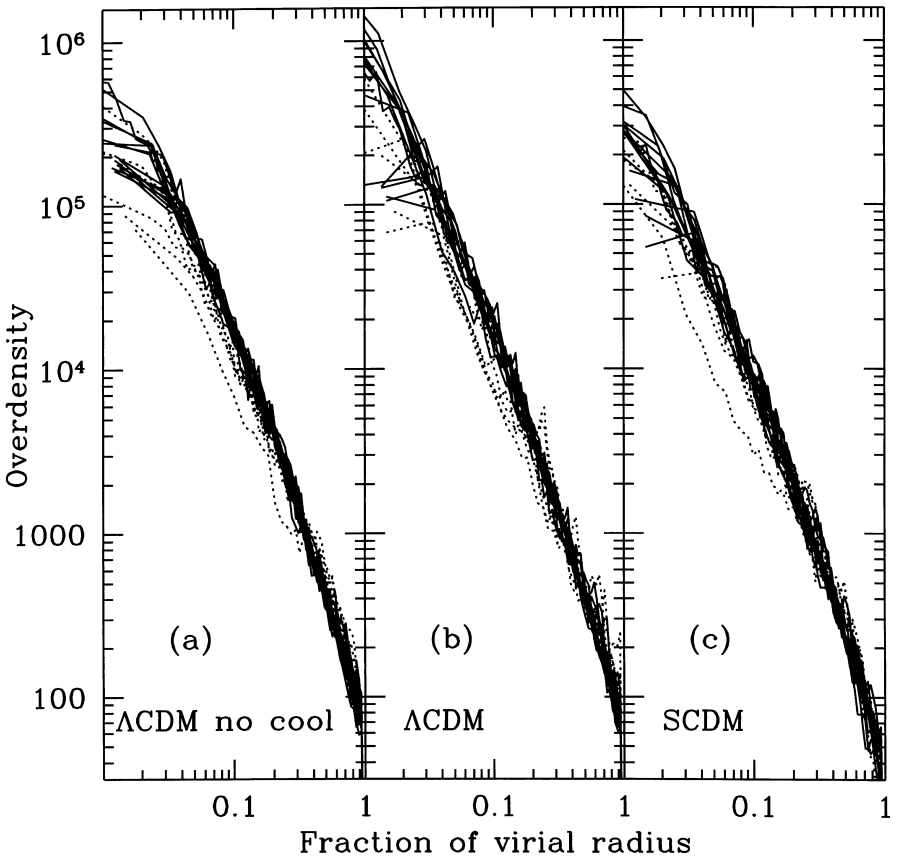

Figure 1. The radial dark matter density profiles of the 20 largest, distinct dark matter haloes extracted from each of the three simulations. Plotted is the mean density within successive spherical shells. Each profile has been scaled to the virial radius and overdensity relative to the cosmic mean for the dark matter. Those profiles marked as dotted lines are for clusters that contain significant substructure (see text). All the profiles are started from the point where 32 particles are enclosed.

similar in each case – this is because cooling has had little effect at these large radii. Between the virial radius and about 0.2 times the virial radius (less for the largest cluster), the entropy profiles for the cooling run are shallower than in the non-cooling run. This confirms the hypothesis of Thomas & Couchman (1992) that cooling is able to *raise* the entropy of the intracluster medium by dragging in high-entropy material from the outer regions of the cluster.

Within about 0.2 virial radii, the entropy profiles again steepen – it is within this 'cooling radius' that the cooling time is short enough to allow significant cooling of the gas within the lifetime of the cluster. By the time we get to the innermost bins in the figure, there seems to be a spread in the entropy of the clusters in the cooling run, with some having higher entropy and some lower entropy than the corresponding clusters in the non-cooling run.

The SCDM run with cooling exhibits similar entropy profiles to the ΛCDM run with cooling.

3.4 Gas density profiles

The radial gas density profiles are displayed in Fig. 4. Without cooling, these profiles look very similar to those obtained by Eke et al. (1998). Within about 0.1 virial radii, the gas profiles are significantly shallower than the corresponding dark matter profiles of Fig. 1. This is indicative of the fact that the hot gas has a higher specific energy than the dark matter and, as previous authors have found (e.g. Navarro et al. 1995; Eke et al. 1998), there is more dark matter than gas (relative to the cosmic mean) within the virial radius. There is a general tendency for all the profiles to flatten considerably in the innermost bin. Once again, this is due to inadequate resolution and we do not attach any significance to it.

The effect of cooling is to *lower* the gas density at all radii within the virial radius. The suppression is greatest, a factor of 3, at about 0.1 times the virial radius, roughly corresponding to the kink in the entropy profiles seen in Fig. 3. Although the density gradients are shallower, they do not roll over into constant-density inner core regions. In fact, for the larger clusters, the density continues to rise further into the centre of the cluster than before, so that the central density is close to that in the non-cooling case.

The profile of the largest object in both gas and dark matter for each of the runs is shown in Fig. 2. The arrow indicates a radius of $100\,h^{-1}$ kpc. Without cooling, the gas density is shallower than that of the dark matter within 0.1 times the virial radius, but this inner, resolved slope of the density profile is still $\rho \propto r^{-1}$ with no sign of a constant-density core. As the temperature is approximately constant within this region (see Fig. 5), the X-ray luminosity is convergent and dominated by emission from around $200\,h^{-1}$ kpc (0.1 times the virial radius).

With cooling, the largest cluster exhibits a central density spike due to the presence of a massive central galaxy. This hot gas has a very steep radial density profile, $\rho \propto r^{-3}$, and would be classified observationally as a cooling flow of $60\,h^{-2}\,\mathrm{M}_{\odot}\,\mathrm{yr}^{-1}$ on to the central cluster galaxy. Between radii of about $40\,h^{-1}$ kpc and $1\,h^{-1}$ Mpc, the density profile is a power law, $\rho \propto r^{-1.4}$,

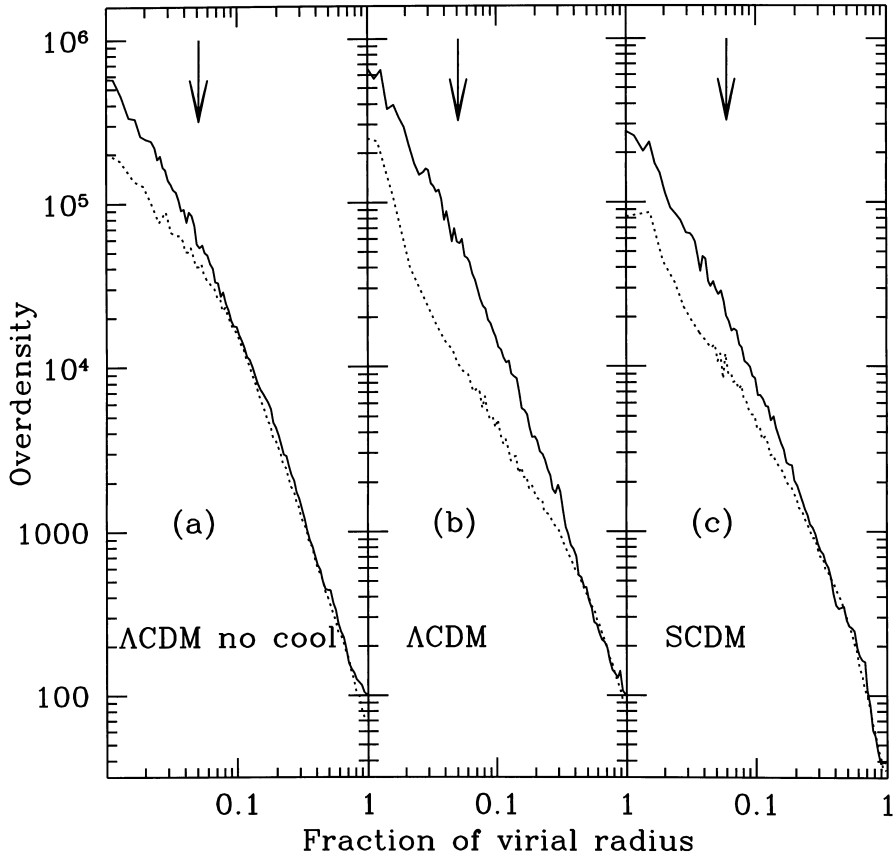

Figure 2. The radial dark matter (solid line) and gas (dotted line) density profile within the virial radius of the largest dark matter halo extracted from each simulation. Each curve is scaled to the virial radius of the halo and overdensity of the appropriate phase relative to the mean cosmic density of that phase. In all three runs there is less gas within the virial radius than dark matter, relative to the cosmic mean of each species. No constant density core is found in the cooling runs. The arrow indicates a scale of $100\,h^{-1}$ kpc.

steepening at larger radii. Thus the X-ray luminosity (excluding the cooling flow) comes from a much more extended region than in the non-cooling case.

In conclusion, the gas density has been reduced by the influx of high-entropy material, as expected. However, this has not given rise to constant-density inner cores. In fact, if anything, the density profiles now continue as a power law closer into the centre of the clusters.

3.5 Radial temperature profiles

Radial temperature profiles are shown in Fig. 5. The temperature profiles for the relaxed clusters from the ΛCDM run without cooling are typical of those found in previous work (see, for example, Eke et al. 1998 and references therein). They rise inwards from the virial radius by about a factor of 2, peaking at about 0.1 times the virial radius and then declining again, very gradually, in the cluster centre.

Cooling makes little difference to the temperature profiles, except that corresponding clusters in the ΛCDM runs reach a *higher* peak temperature when cooling is implemented, due to the inflow of higher-entropy gas. The temperatures are very similar at the virial radius, but are about 1.5 times higher at their peak than before. Two clusters show a precipitous decline in temperature in the cluster centre, one of these being the largest cluster – this is evidence for a cooling flow.

The SCDM results are very similar to those for ΛCDM.

3.6 X-ray luminosity profiles

We follow Navarro et al. (1995) in using the following estimator for the bolometric X-ray luminosity of a cluster,

$$L_{\rm X} = 4\times10^{32}\sum\left(\frac{\rho_i}{\bar{\rho}}\right)\left(\frac{T_i}{\rm K}\right)^{1/2}\ {\rm erg\,s^{-1}} \qquad (1)$$

where the density is in units of overdensity (relative to the mean gas density in the box, $2.86\times10^{-31}\,{\rm g\,cm^{-3}}$) and the sum extends over all the gas particles with temperatures above 12 000 K.

The total X-ray luminosity within the virial radius of each of the clusters is listed in Tables 2–4. For the simulation with cooling the clusters are several times less luminous than those from the corresponding non-cooling run. This contradicts the previous results of Katz & White (1993), Suginohara & Ostriker (1998) and Lewis et al. (2000) who all found the X-ray luminosity increased if cooling was turned on. The reason for the discrepancy is, once again, the fact that we have decoupled the hot and cold gas, thus greatly suppressing the cooling of the inflowing, high-entropy gas in our simulations compared to previous ones. This causes a large reduction in the mass of the brightest cluster galaxy compared to those produced by previous work. Our galaxies have reasonable luminosities, mass-to-light ratios and number counts for a volume of this size.

Note that estimates of X-ray luminosity from the non-cooling run are not really meaningful. A radiation rate of this magnitude

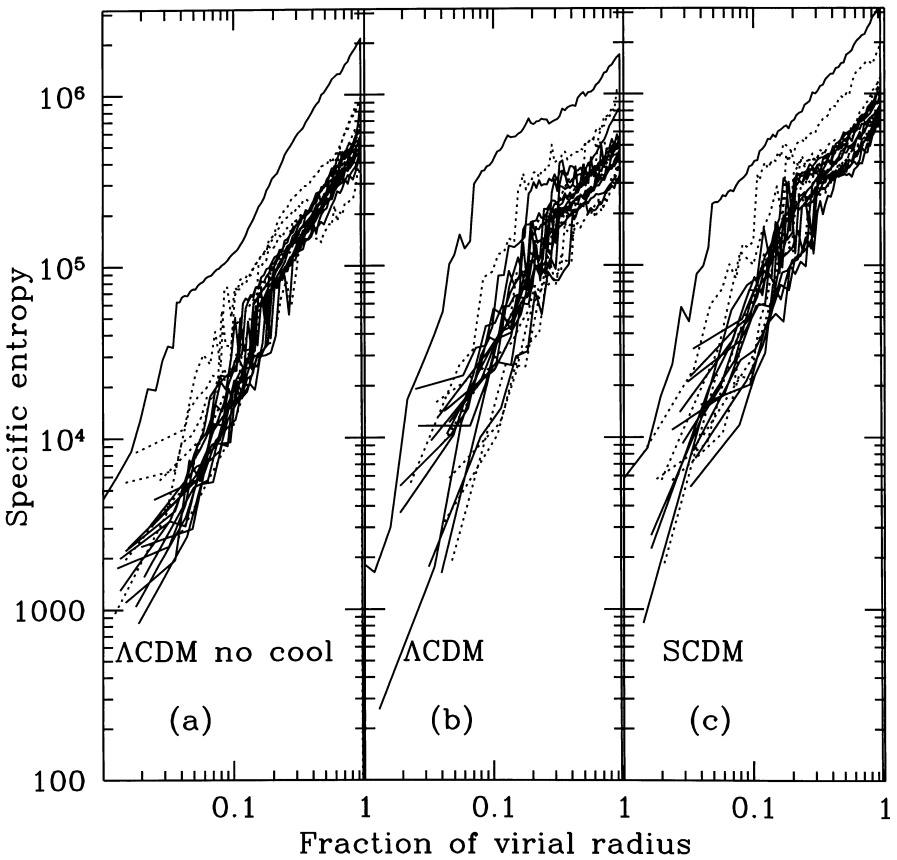

Figure 3. The radial specific entropy profiles of the 20 largest, distinct haloes extracted from each of the three simulations. Plotted is the mean value of $T/n^{2/3}$ within successive spherical shells. Each profile has been scaled to the virial radius. Those profiles marked as dotted lines are for clusters that contain significant substructure (see text).

can only be sustained for a short time before depleting the intracluster medium of gas. The cooling runs produce a more physically self-consistent X-ray luminosity because the radiative effects are taken into account. The X-ray luminosity within the cooling radius is approximately equal to the enthalpy of the gas divided by the age of the cluster.

We plot these bolometric luminosities as a function of radius for each of our clusters in Fig. 6. Clearly, the relative contribution to the total X-ray emission from different radii is very different for the cooling and non-cooling simulations. Without cooling all the relaxed clusters show very similar emission profiles, with only a small contribution to the total emission coming from the very centre. These profiles are mostly well resolved, as claimed by Eke et al. (1998) for simulations of clusters with this particle number.

Once radiative cooling is turned on, the radial emission profiles span a much broader range. For two of the clusters, a central cooling-flow-type emission is clearly visible – contributing 50 and 80 per cent of the total X-ray flux. Although the cooling flow region is not well resolved, it cannot be much larger without depleting the intracluster medium of even more gas. For each of the other clusters, the radius enclosing half of the total emission is much larger than that for the simulation without cooling.

3.7 L_X–T_X relation

There has been much debate in the literature centering on the X-ray cluster L_X versus T_X correlation. The emission weighted mean temperature is plotted against the bolometric luminosity within the virial radius for all our clusters in Fig. 7. The filled symbols represent the relaxed clusters and the open symbols denote those clusters that show significant substructure.

The effect of cooling is, in general, to slightly raise the temperature but to greatly reduce the X-ray luminosity. Exceptions are the cooling flow clusters where the large amount of emission from gas cooling on to the central galaxy gives rise to a lower temperature than in the non-cooling case. There are two of these, easily visible on the plot, in the ΛCDM run; we have plotted their new locations, when the central cooling flow is omitted, using crosses linked to the old location via arrows. In both cases less than 2 per cent of the hot, X-ray emitting particles were excised to make this calculation (606 for cluster Λ1 and 20 for cluster Λ5). In the case of Λ5 we have caught a transient event – a small amount of gas has been reheated by a merger between a satellite and the brightest cluster galaxy. This gas is in the process of rapidly cooling back on to the central object, emitting large amounts of X-rays.

All three sets of clusters display a positive correlation between L_X and T_X, although there are insufficient numbers to tie the trend down very tightly. It is clear from the comments in the preceding paragraph that the nature of the correlation depends critically upon whether one removes the cooling flow emission or not. We believe that a clearer picture arises if this is done.

The regression line in Fig. 7 is from Eke et al. (1998) and corresponds to $L_X \propto T_X^2$. Our non-cooling clusters fit reasonably well with this relation. The cooling clusters lie below this line.

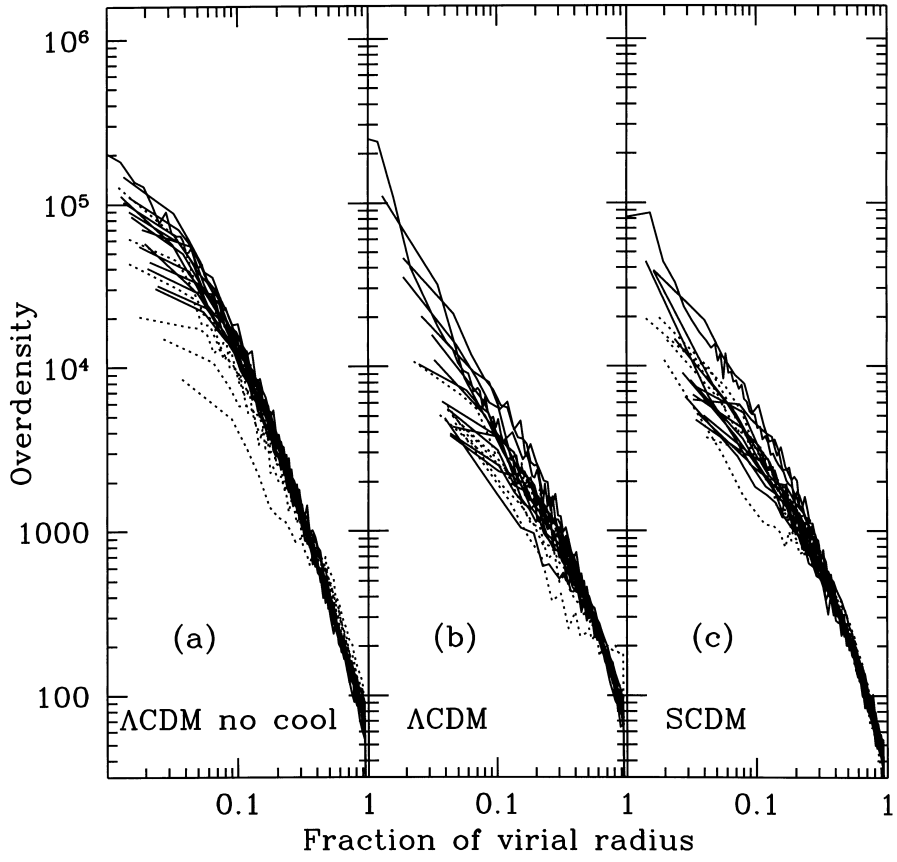

Figure 4. The radial gas density profile of the 20 largest haloes found within each simulation. Those haloes containing significant substructure are shown as dotted lines. Plotted is the mean gas density within successive spherical shells. All the haloes are scaled to the virial radius and gas overdensity relative to the baryonic cosmic mean.

Given that we expect cooling to be less important in the most massive clusters (the absolute value of the cooling time and the ratio of the cooling time to the dynamical time both increase with cluster mass), then we would expect the clusters with radiative cooling to lie closer to the regression line at higher T_X. Thus the effect of cooling should be to steepen the L_X–T_X relation. We hope to test this with more simulations of higher mass clusters.

Also plotted in Fig. 7 are the observed data from David et al. (1995). Our clusters are smaller and cooler because they are not very massive (because of our relatively small computational volume), thus it is hard to assess whether the cooling or the non-cooling clusters give a better fit to the data. SCDM clusters, at least with the simulation parameters we have chosen in this paper, do not seem to provide such a good match to the data.

4 CONCLUSIONS AND DISCUSSION

We have performed two *N*-body plus hydrodynamics simulations of structure formation within a volume of side 100 Mpc, including the effects of radiative cooling but neglecting star formation and feedback. By repeating one of the simulations without radiative cooling of the gas, we can both compare with previous work and study the changes caused by the cooling. A summary of our conclusions follows.

(i) Without cooling, our clusters closely resemble those found by previous authors (Eke et al. 1998 and references therein), with dark matter density profiles that closely follow the universal formula proposed by Navarro et al. (1995).

(ii) With cooling, the formation of a central galaxy within each halo acts to steepen the dark matter profile, supporting the conclusion of the lensing studies (e.g. Kneib et al. 1996) that the underlying potential that forms the lens has a small core. This galaxy may not be located exactly at the centre of the X-ray emission, sometimes being offset by up to $50\,h^{-1}$ kpc. The inner slope of the density profile is then steeper than that suggested by NFW, closer to that found by Moore et al. (1998) from high-resolution *N*-body simulations (but note that these did not include cooling gas).

(iii) We confirm the results of Eke et al. (1998) (and previous studies quoted therein) that without radiative cooling the gas density profile turns over at small radii, that the radial temperature profile drops by a factor of 2 between its peak value and that obtained at the virial radius and that the baryon fraction within the virial radius is lower than the cosmic mean.

(iv) Cooling acts to remove low-entropy gas from near the cluster centre, triggering the inflow of higher-entropy material. The entropy excess compared with the non-cooling run is greatest at about 0.2 times the virial radius, because radiative cooling lowers the entropy of the gas near the centre of the cluster.

(v) We stress the importance of correctly modelling the central cluster galaxy. The resultant X-ray properties of the cluster are very dependant upon the centre and if too much material cools into the base of the potential well, large amounts of hot, dense gas

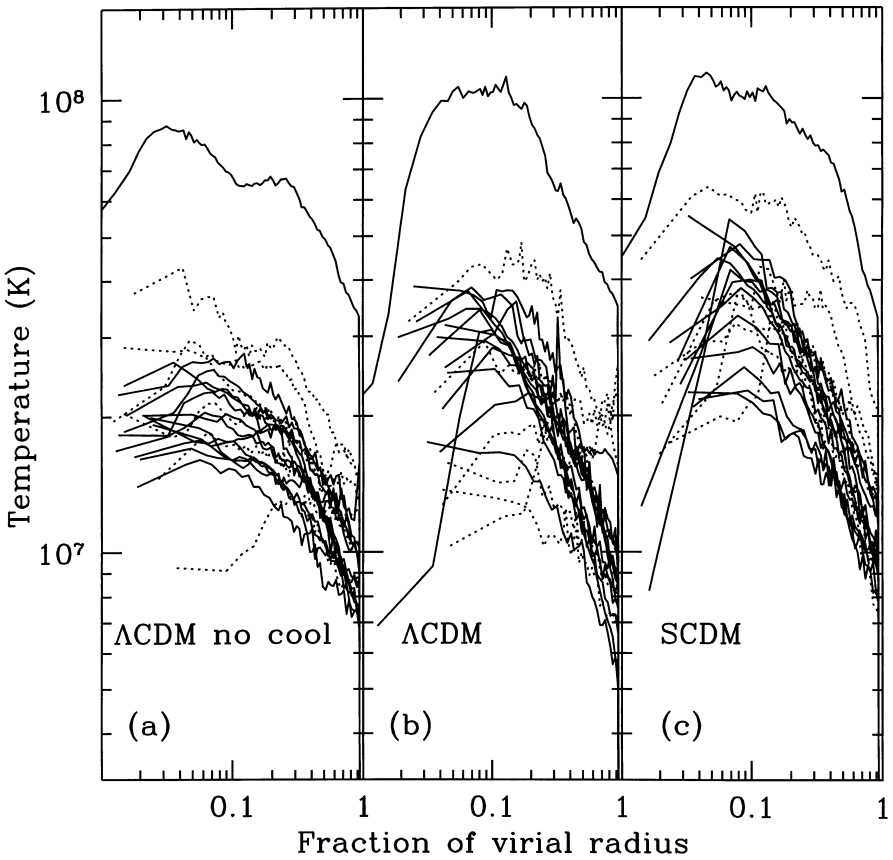

Figure 5. The radial gas temperature profile found within each of the 20 haloes extracted from each cosmology. Clusters with significant substructure are marked as dotted lines. All the haloes are scaled to the virial radius and temperatures (calculated as the mass-weighted mean temperature of the gas within successive spherical shells) are in Kelvin. With cooling the cluster temperature reaches a slightly higher maximum at a larger fraction of the virial radius, whereas the temperature at the virial radius is very similar.

can be confined, producing enormous X-ray fluxes. We have specifically tailored our models to both globally cool a reasonable fraction of material and to circumvent problems encountered by SPH when faced with large density jumps, which can lead to high rates of gas cooling on to the central objects.

(vi) In cooling clusters, the gas density is reduced, by a maximum of about a factor of 3 at 0.1–0.2 times the virial radius. The density profile more closely resembles a power law than in the non-cooling run. A few clusters show a central density spike, indicative of a cooling flow on to the central cluster galaxy (e.g. Fabian, Nulsen & Canizares 1991).

(vii) The temperatures of the cooling clusters show a significant fall between the point where the peak values are obtained (around 0.1 virial radii) and the virial radius. The observational evidence is somewhat divided here. Our results are in agreement with Markevitch et al. (1998), who find that the temperature profile of galaxy clusters are steeply falling. However, Irwin et al. (1999) recover isothermal temperature profiles out to the virial radius from an averaged sample of 26 *ROSAT* clusters. It is important to try to clear up this observational controversy as isothermal temperature profiles are not seen in our models, but are often used for X-ray mass estimates, measurements of Ω_b (and hence Ω) and theoretical arguments for the L_X–T_X relation.

(viii) Cooling acts so as to *increase* both the mass-weighted and observed X-ray temperatures of clusters. The peak temperatures are raised by a factor of about 1.5 and the temperature gradient between the peak and the virial radius is correspondingly increased.

(ix) The bolometric luminosity for the clusters with radiative cooling is around 3–5 times *lower* than for matching clusters without it. Except for the cooling flow clusters, the X-ray luminosity profile is less centrally concentrated than in the non-cooling case with a greater contribution coming from larger radii.

(x) Cooling flow clusters are easily distinguished from non-cooling flow clusters in the L_X–T_X plane. The former are more luminous and cooler than the latter (Fabian et al. 1994; Allen & Fabian 1998). Some of this difference results from X-ray analysis methods (Allen & Fabian 1998) but may also be caused by actual physical differences in the mass distribution of clusters. We suggest that, while interpretation of this relation would be made simpler if the cooling flow were excluded before determining the X-ray properties of clusters, this should be done with caution.

(xi) The clusters from the non-cooling simulation lie on the $L_X \propto T_X^2$ regression line of Eke et al. (1988), whereas those from the cooling run lie below it. We suggest that, as cooling is likely to be less important in more massive clusters, the effect of cooling will be to steepen the relation. This remains to be tested with simulations of more massive clusters.

(xii) The very large core radii ($\sim 250\,h^{-1}$ kpc) observed in some clusters are not seen in our simulations. It is possible that such events are rare, or occur preferentially in massive clusters, in which case our cluster sample may simply be too small to contain such objects. Smaller core radii of around $\sim 50\,h^{-1}$ kpc are close to our resolution limit and so are not ruled out by our results, although we find no evidence for a constant-density region in the centre of any of our clusters.

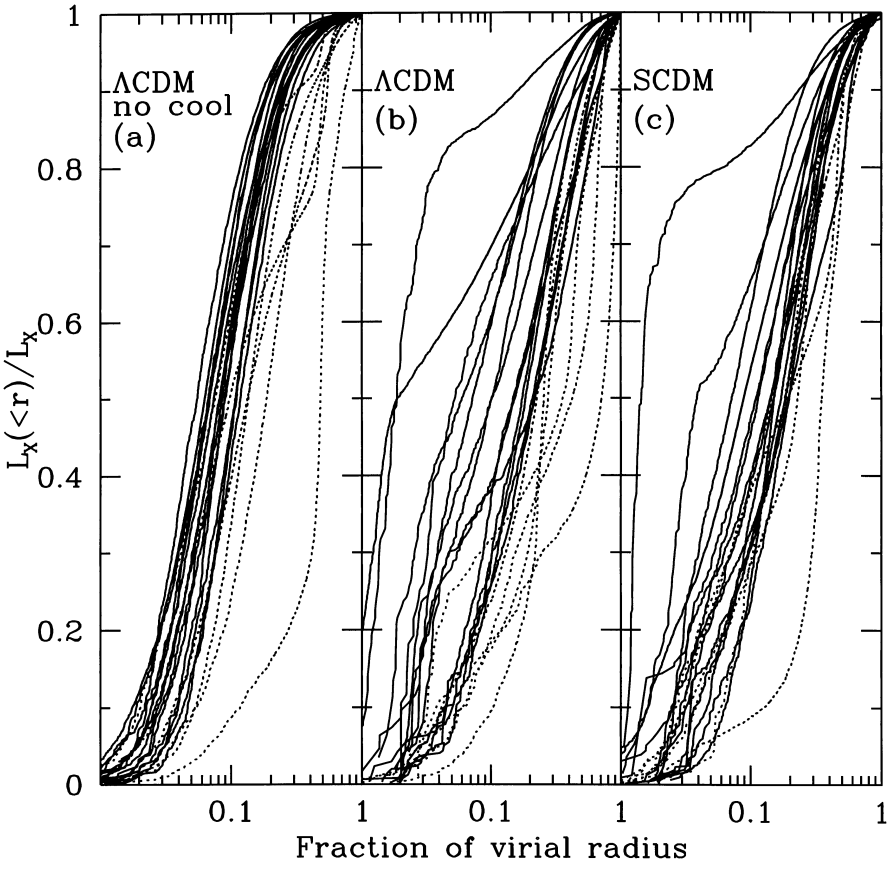

Figure 6. The fraction of the total bolometric luminosity that is emitted from within the specified radius for each of the clusters (calculated from equation 1). Clusters with significant substructure are shown as dotted lines.

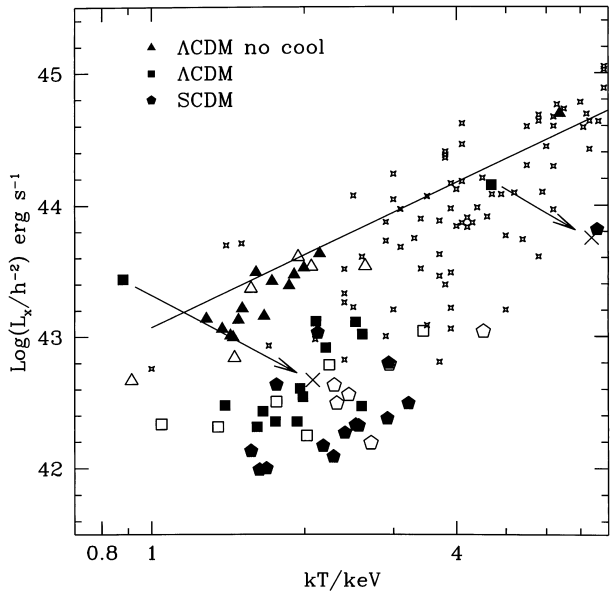

Figure 7. The luminosity–temperature relation for all the clusters. Open symbols refer to those clusters with significant substructure, filled to those without. The small symbols are the observation data from David, Jones & Forman (1995). The majority of our clusters are small because the simulation volume is only 100 Mpc on a side but span a reasonable range. The values plotted are the emission weighted mean temperature converted to keV and the bolometric luminosity within the virial radius. The regression line is that of Eke et al. (1998), figure 16. and represents a fit to the X-ray luminosity of their ΛCDM clusters. The crosses show where the two ΛCDM clusters indicated would appear on the diagram if their central cooling flow emission was removed from both the bolometric X-ray and emission weighted temperature calculations.

At this point, we should remind the reader that our simulations are designed merely to investigate the effect of radiative cooling on the X-ray properties of the intracluster medium and do not set out to explore the complete range of physical processes going on in clusters. In particular, we ignore the possibility of energy injection into the intracluster medium. Early star formation at high redshift and the subsequent energy feedback from supernovae could act to preheat the gas which falls into the potential wells of galaxy clusters, effectively raising its entropy to such a level that it cannot reside at the high densities required to trace the dark matter into the base of the potential well, and giving rise to the constant-density cores that our simulated clusters lack. Ponman, Cannon & Navarro (1999) argue for such preheating by examining ROSAT observations of 25 clusters.

The inclusion of cooling into a cosmological hydrodynamics simulation has proved highly successful. We have highlighted the necessity of cooling reasonable amounts of gas on to the centre of each galaxy cluster if sensible X-ray luminosity estimates are to be obtained. We have achieved this by a judicious choice of mass resolution and decoupling the hot and cold gas phases. A rigorous method of doing this in SPH is under development. We next intend to simulate more massive clusters in the same way, in order to extend our predictions into regions more accessible to observation.

ACKNOWLEDGMENTS

The work presented in this paper was carried out as part of the programme of the Virgo Supercomputing Consortium using computers based at the Computing Centre of the Max-Planck Society in Garching and at the Edinburgh Parallel Computing Centre. The authors thank NATO for providing NATO Collaborative Research Grant CRG 970081 which facilitated their interaction and the anonymous referee for suggesting significant improvements. PAT is a PPARC Lecturer Fellow.

REFERENCES

Allen S. W., 1998, MNRAS, 296, 392
Allen S. W., Fabian A. C., 1998, MNRAS, 297, L57
Abramopoulos F., Ku W.H.-M., 1983, ApJ, 271, 446
Bartelmann M., Steinmetz M., 1996, MNRAS, 283, 431
Beers T. C., Tonry J. L., 1986, ApJ, 300, 557
Bower R. G., 1997, MNRAS, 288, 355
Bryan G. L., Cen R., Norman M. L., Ostriker J. P., Stone J. M., 1994, ApJ, 428, 405
Bryan G. L., Norman M. L., 1998, ApJ, 495, 80
Cen R., Ostriker J. P., 1994, ApJ, 429, 4
Copi C. J., Schramm D. N., Turner M. S., 1995, ApJL, 455, L95
Couchman H. M. P., 1991, ApJL, 368, L23
Couchman H. M. P., Thomas P. A., Pearce F. R., 1995, ApJ, 452, 797
David L. P., Jones C., Forman W., 1995, ApJ, 445, 578
Edge A. C., Stewart G. C., Fabian A. C., Arnaud K. A., 1990, MNRAS, 245, 559
Eke V. R., Cole S., Frenk C. S., 1996, MNRAS, 282, 263
Eke V. R., Navarro J. F., Frenk C. S., 1998, ApJ, 503, 569
Evrard A. E., 1990, ApJ, 363, 349
Evrard A. E., Metzler C. A., Navarro J. F., 1996, ApJ, 469, 494
Evrard A. E., Summers F. J., Davis M., 1994, ApJ, 422, 11
Fabian A. C., Crawford C. S., Edge A. C., Mushotzky R. F., 1994, MNRAS, 267, 779
Fabian A. C., Nulsen P. E. J., Canizares C. R., 1991, A&AR, 2, 191
Frenk C. S., Evrard A. E., White S. D. M., Summers F. J., 1996, ApJ, 472, 460
Frenk C. S. et al., 1999, ApJ, 525, 554
Gardner J. P., Sharples R. M., Frenk C. S., Carrasco E., 1997, ApJ, 480, 99
Gerritsen J. P. E., Icke V., 1997, A&A, 325, 972
Gingold R. A., Monaghan J. J., 1977, MNRAS, 181, 375
Irwin J. A., Bregman J. N., Evrard A. E., 1999, ApJ, 519, 518
Jenkins A. et al., 1998, ApJ, 499, 20
Jones C., Forman W., 1984, ApJ, 276, 38
Kang H., Cen R., Ostriker J. P., Ryu D., 1994, ApJ, 428, 1
Katz N., 1992, ApJ, 391, 502
Katz N., White S. D. M., 1993, ApJ, 412, 455
Kneib J.-P., Ellis R. S., Smail I., Couch W. J., Sharples R. M., 1996, ApJ, 471, 643
Lewis G. F., Babul A., Katz N., Quinn T., Hernquist L., Weinberg D. H., 2000, ApJ, 536, 623
Lucy L. B., 1977, ApJ, 82, 1013
Markevitch M., Forman W. R., Sarazin C. L., Vikhlinin A., 1998, ApJ, 503, 77
Metzler C. A., Evrard A. E., 1994, ApJ, 437, 564
Mihos J. C., Hernquist L., 1994, ApJ, 437, 611
Moore B., Governato F., Quinn T., Stadel J., Lake G., 1998, ApJL, 499, L5
Navarro J. F., Frenk C. S., White S. D. M., 1995, MNRAS, 275, 720
Navarro J. F., Frenk C. S., White S. D. M., 1997, ApJ, 490, 493
Navarro J. F., White S. D. M., 1994, MNRAS, 267, 401
Pearce F. R. et al., 1999, ApJ, 521, L99
Pearce F. R., Couchman H. M. P., 1997, New Astron., 2, 411
Pearce F. R., Thomas P. A., Couchman H. M. P., 1993, MNRAS, 264, 497
Peres C. B., Fabian A. C., Edge A. C., Allen S. W., Johnstone R. M., White D. A., 1998, MNRAS, 298, 416
Ponman T. J., Cannon D. B., Navarro J. F., 1999, Nature, 397, 135
Steinmetz M., White S. D. M., 1997, MNRAS, 288, 545
Suginohara T., Ostriker J. P., 1998, ApJ, 507, 16

Thomas P. A.,et al., 1998, MNRAS, 296, 1061
Thomas P. A., Couchman H. M. P., 1992, MNRAS, 257, 11
Waxman E., Miralda-Escude J., 1995, ApJ, 451, 451
White D. A., Jones C., Forman W., 1997, MNRAS, 292, 419
White S. D. M., Rees M. J., 1978, MNRAS, 183, 341
Wu K. K. S., Fabian A. C., Nulsen P. E. J., 1998, MNRAS, 301, L20

This paper has been typeset from a TEX/LATEX file prepared by the author.